CORA Cork Open Research Archive
Cartlann Taighde Oscailte Chorcaí

Title	Process of formation of porous layers in n-InP
Authors	Quill, Nathan;Clancy, Ian;Nakahara, Shohei;Belochapkine, Serguei;O'Dwyer, Colm;Buckley, D. Noel;Lynch, Robert P.
Publication date	2017-05-01
Original Citation	Quill, N., Clancy, I., Nakahara, S., Belochapkine, S., O'Dwyer, C., Buckley, D. N. and Lynch, R. P. (2017) 'Process of Formation of Porous Layers in n-InP', ECS Transactions, 77(4), pp. 67-96. doi: 10.1149/07704.0067ecst
Type of publication	Article (peer-reviewed)
Link to publisher's version	http://ecst.ecsdl.org/content/77/4/67.abstract - 10.1149/07704.0067ecst
Rights	© 2017 ECS - The Electrochemical Society
Download date	2026-11-05 23:57:01
Item downloaded from	https://hdl.handle.net/10468/6172



University College Cork, Ireland
Coláiste na hOllscoile Corcaigh

Formation Process of Pores Layers in n-InP

N. Quill,[a] I. Clancy,[a] C. O'Dwyer,[b] S. Nakahara,[a] S. Belochapkine,[a] D. N. Buckley [a] and R.P. Lynch[a]

[a] Department of Physics, and Bernal Institute, University of Limerick, Ireland

[b] Department of Chemistry, and Tyndall National Institute, University College Cork, Ireland

Abstract

This paper describes variations in current density observed in linear sweep voltammetry curves during the anodization of n-InP in aqueous KOH electrolyte and how they arise. This analysis is performed by stopping the anodization after different durations of etching and observing via scanning electron microscopy the porous structures that have been formed. A mathematical model for the expansion and merging of domains of pores that propagate preferentially along the <111>A directions is also presented and utilised to explain the previously mentioned variations in current density.

INTRODUCTION

The anodic formation of porosity in semiconductors has received considerable attention, due to the fundamental insight it offers into semiconductor etching properties and its wide range of possible applications [1]. Although a number of models have been proposed to explain the formation of porosity in semiconductors [2-5], none as yet can explain the complete range of structures which have been formed in different semiconductor-electrolyte systems.

The anodic etching of n-type semiconductors in the dark is limited by hole supply at the semiconductor surface. It is generally accepted that this limited hole supply is what causes the initiation and propagation of porous etching, with hole supply being enhanced (and hence, porous etching initiated) at defect sites at the surface [6]. The newly formed pore tips then act as sites for the continuous preferential supply of holes [7]. However, the variation in feature size, as well as the morphology observed, as experimental conditions are varied cannot be so readily explained.

We have previously investigated [8,9] the early stages of anodic formation of porous InP in 5 mol dm^{-3} KOH and reported transmission and scanning electron microscopy (TEM and SEM) evidence that clearly show individual nanoporous domains. From this work we concluded that pore propagation was preferentially along the <111>A direction. [10] This porosity originates from pits in the surface creating domains of pores beneath a thin (~40 nm) dense near-surface layer. [11] The domains that initially form have triangular $(01\bar{1})$ cross-sections, 'dove-tail' (011) cross-sections and rectangular profiles when viewed in (100) planes parallel to the electrode surface. [12,13] Each domain is connected to the surface via an individual channel, and eventually these domains merge to form a continuous porous layer, beneath the dense near-surface layer. [14] It was also observed by our group [15-17] that these structures are obtained when InP is anodized in KOH at concentrations of 2 mol dm^{-3} or above. However, at concentrations of 1 mol dm^{-3} or less, no porous layers were observed and between 1.8 mol dm^{-3} and 1.0 mol dm^{-3} a transitional behaviour that exhibits highly porous growth (without the presence of a near surface layer) was observed. Furthermore, we have developed a mechanism [18], based on our results for pore formation in n-InP in KOH, in which the variations in pore morphology are due to the competition in kinetics between hole supply, carrier diffusion at the semiconductor surface and electrochemical.

In this paper, relationships between the current in linear sweep voltammograms (LSVs) from experiments preformed with 5 mol dm^{-3} KOH and the detailed etching processes that result are investigated. Electrochemical and microscopy results will be presented and surface pit densities, merging of porous domains to form continuous porous layers, porous layer depths and the expansion and termination of expansion of these layers will be related to and explained by characteristics that are observed in the LSVs. These results are further supported by a mathematical model that is based on the expansion and merging of the porous domains formed by <111>A pore growth.

EXPERIMENTAL

Unless otherwise stated, the working electrode consisted of polished (100)-oriented monocrystalline sulphur-doped n-type indium phosphide (n-InP). An ohmic contact was made to the back of the InP sample and isolated electrically from the electrolyte by means of a suitable varnish. The electrode area was typically 0.5 cm^2. InP wafers with carrier concentrations from 3.4×10^{18} to 6.7×10^{18} cm^{-3} and etch pit densities of less than 500 cm^{-2}

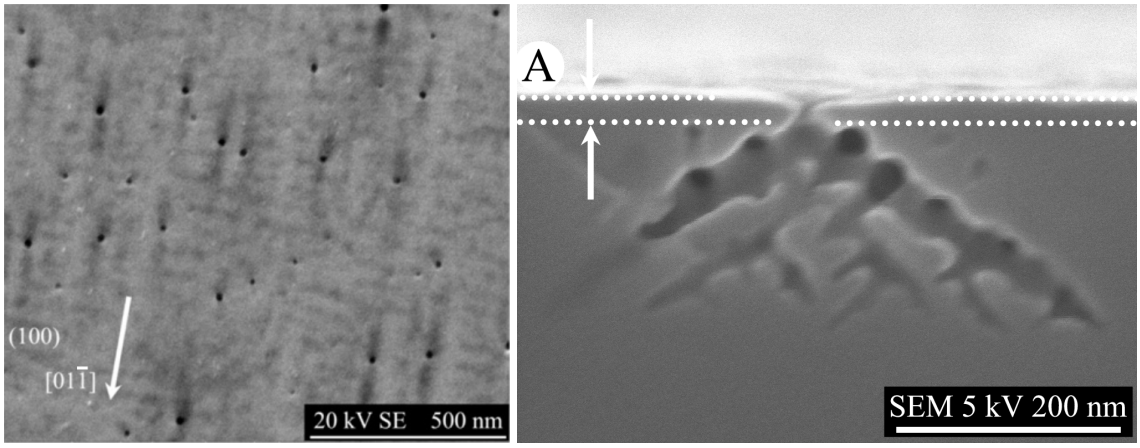
were used. Anodization was carried out in aqueous KOH electrolytes of 5 mol dm^{-3}. Each experiment involved a linear potential sweep (LPS) from 0.0 V (SCE) to an upper potential at 2.5 mV s^{-1}. A conventional three-electrode cell configuration was used employing a platinum counter electrode and saturated calomel reference electrode (SCE) to which all potentials were referenced. Prior to immersion in the electrolyte, the working electrode was dipped in an etchant (3:1:1 H_2SO_4:H_2O_2:H_2O) for 4 minutes and then rinsed in deionized water. All of the electrochemical experiments were carried out in the absence of light at room temperature.

A CH Instruments Model 650A Electrochemical Workstation interfaced to a Personal Computer (PC) was employed for cell parameter control and for data acquisition. Cleaved {011} cross-sections were examined using a Hitachi S-4800 field-emission scanning-electron-microscope (SEM) operating at 5 kV. Electron transparent sections for cross-sectional transmission electron microscope (TEM) examination were prepared using standard focused ion beam milling (FIB) procedures [19] in a FEI 200 FIB workstation. The TEM characterization was performed using a JEOL JEM 2010 TEM operating at 200 kV.

RESULTS AND DISCUSSION

Relationship of Linear Potential Sweeps and Pore Growth

When an anodic potential is applied to an n-type InP electrode, a region near the surface is depleted of carriers. This region of fixed space charge prevents etching since the semiconductor is unable to conduct carriers to the electrolyte interface. Where defects arise on the electrode surface, variations in the energy levels of the surface state (due to defects and surfaces ledges) or variations in the space charge layer width (perhaps due to a local perturbation of the doping density) can allow localised etching to occur. This localised etching leads to the formation of surface pits. At these pits the electric field is magnified due to the high surface-curvature of the pit walls. [10] Under these conditions quantum tunnelling of holes from the valence band – due to the pits acting as centres of high electric-field – results in increased localised etching at the surface pits. These pits (Fig. 1a) then act as the source of pore growth which spreads into the bulk semiconductor leaving an almost intact near-surface layer of dense InP (Fig. 1b at A) where the fixed space charge layer exists. [13] Each pit produces an individual domain of pores that are linked back through it to the surface. It should be noted that such pore growth does not occur for electrodes of carrier concentration less then 10^{17} cm^{-3} (as shown by the observations of little current density being passed for such samples and TEM evidence in the work of O'Dwyer. [20])



(a) (b)

Fig. 1 (a) SEM micrograph of an InP (100) surface (n = 3.4 x 10^{18} cm^{-3}) following a LPS from 0.0 to 0.537 V (SCE). Since the image was taken at 20 kV both the surface pits and some sub-surface features are shown. (b) SEM micrograph of (011) cleavage plane following a LPS from 0.0 to 0.245 V (SCE) (n = 5.3 x 10^{18} cm^{-3}) showing the cross-sections of a young porous domain that has not already merged, growing from a pit in the surface beneath a near-surface layer of dense InP (at A).

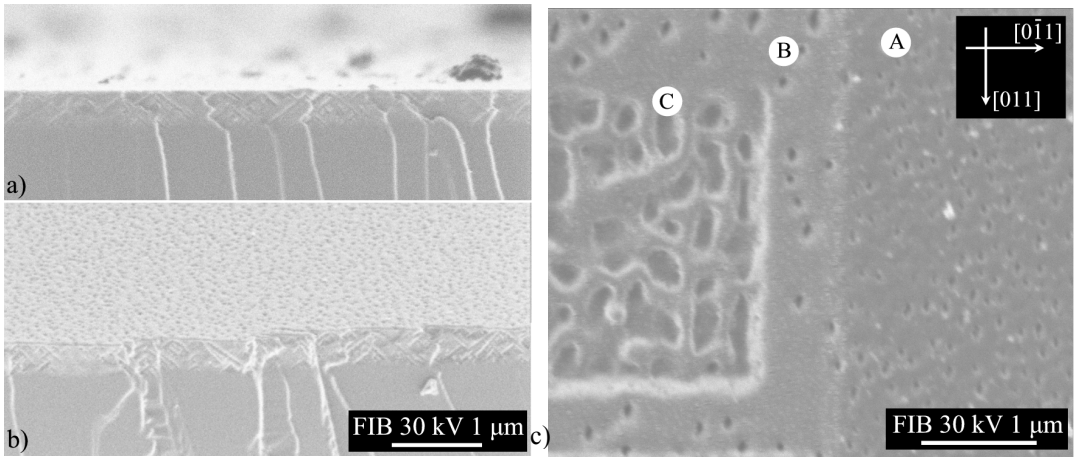


Fig. 2 FIB images of the (a) (011) cross-section of an InP sample (n = 3.4 x 10^{18} cm^{-3}) anodized at 0.3 V (SCE) for 600 s and (b) the same sample tilted so as to see the surface of the electrode. The surface pits and other features shown in b are wider than their original values due the ion beam milling due imaging of the area 23 times. (c) FIB image of the (100) InP electrode surface of the same sample. Three different depths into the surface are shown which resulted from ion beam milling as each region (A) once, (B) 15 times and (C) 30 times. The <011> directions shown in the inset were calculated from the orientation of the primary and secondary flats of the wafer.

Focused Ion Beam (FIB) Images of Porous Growth

Fig. **2**a and 2b show a FIB images of an InP electrode that has been cleaved along the (011) plane after anodization at 0.3 V for 600 s. This voltage is above the potential required for pit formation to occur and it can be observed in Fig. 2a that a continuous porous-layer has formed. Since the ion beam in the FIB peels the surface away by milling atoms away it is possible to widen the features and to see the porous layer more clearly. Fig. **2**b shows an image of the same sample after it has been tilted and 23 images have been taken. As can be seen this repeated imaging has widened/formed pits in the electrode surface (i.e. the top half of the image) but also clearly shows that a layer is observable below the surface.

When repetitive scans are preformed on the same area the way the surface changes due to the removal of layers of atoms by the FIB can be observed as the images progress. Fig. **2**c shows an FIB image that uses repetitive imaging to mill away layers of the electrode. Three different regions, of increasing depth into the sample, can clearly be seen in the image at A, B and C, corresponding to the area in that region being subjected to 1, 15 and 30 exposures, respectively. Region A shows a large density of pits on the surface which is higher than the corresponding density of pits seen in SEM micrographs. Therefore these pits do not correspond to the surface pits formed during the anodization but to damage by the ion beam. Region B shows a deeper image where these pits have been widened slightly while Region C shows how the porosity of the sample suddenly increases when the FIB has milled through the near-surface layer of dense InP to where the electrochemical etching has formed pores. It can also be seen in Region C that, where the pores are extended along a direction this direction tends to be one of the two orthogonal <011> directions – in agreement with the regular mesh that is predicted by the analysis of <111>A pore growth [10].

Scanning Electron Microscope Images of Porous Growth

Normally n-type materials are not expected to etch anodically under dark conditions but at strong positive potentials quantum tunnelling of holes in the valence band can allow etching to occur. Fig. **3** shows a typical linear sweep voltammogram (LSV) for a sample of InP with a carrier concentration of $n = 3.4 \times 10^{18}$ cm^{-3}. The LSV displays a large current density, which peaks at 0.46 V corresponding to the etching of InP and the creation of a porous layer. The graph has been split up into several regions and there are also four positions − α, β, γ and δ − indicated on the current density curve corresponding to the four SEM images shown in Fig. 4. As can be seen in the LSV there is one current peak (at β, *i.e.* at $E_{p1,2}$) but as will be

shown later at higher carrier concentrations there can be more than one peak; *i.e.* at this carrier concentration, this single peak is the concurrence of two aspects of the etching mechanism and at higher carrier concentrations, as will be shown later, these aspects of the mechanism result in distinguishable peaks.

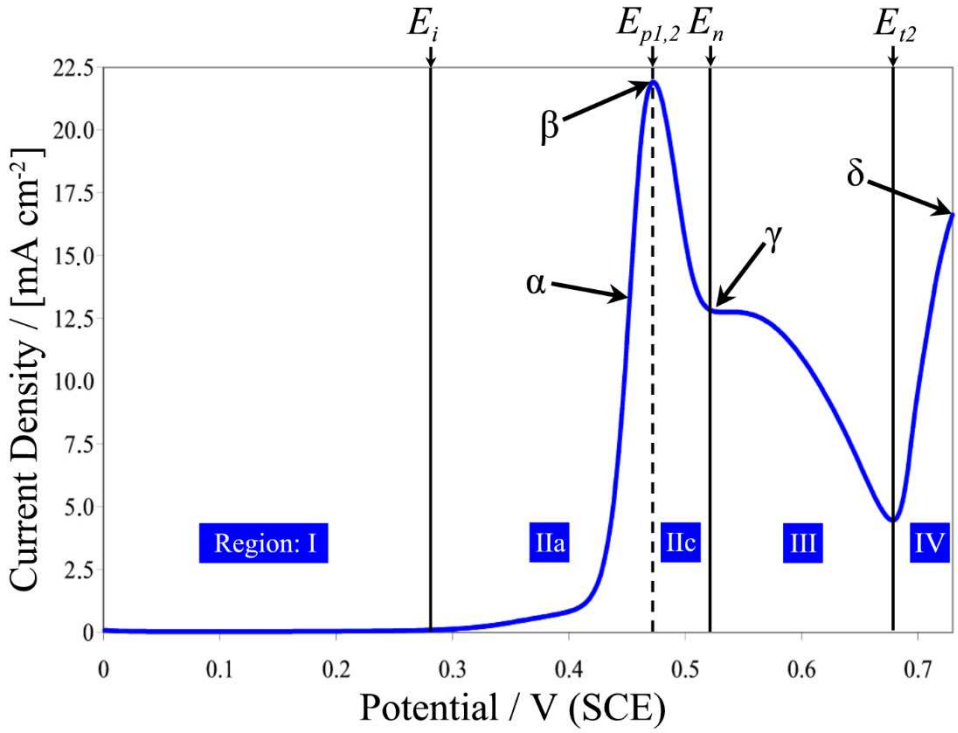


Fig. 3 LSV for InP (n = 3.4 x 10^{18} cm^{-3}) from 0 to 0.73 V (SCE) at 2.5 mV s^{-1} in 5 mol dm^{-3} KOH in darkness at room temperature. The graph is divided into five regions of differing behaviour of which the controlling mechanism is discussed. Also shown are the positions of SEM micrographs a, b, c and d (Fig. 4).

In Region I of Fig. 3 very little etching occurs since the initiation potential, E_i, required for pit formation on the surface has not been achieved. Once E_i has been achieved (>0.28 V) pits start to form in the surface and from these pits sub-surface domains of pores spread out beneath the surface (Fig. 4α).

As described previously [10], the shapes of the domains formed are the result of pore growth occurring solely along the <111>A crystallographic directions. These domains have a truncated tetrahedral shape and as they grow in number and size the number of active pore tips increases, increasing the surface area being etched and therefore increasing the current density (Region IIa of Fig. 3). After an extended duration of etching a continuous porous layer is observed beneath the thin dense near-surface layer (Fig. 4β). As the domains merge

to create this continuous porous layer the number of tips saturates as merging is completes. Once the continuous porous layer is created the crystallographic growth continues (note: this part of the process – *i.e.* Region IIb – is not present in Fig. 3 since the domains never fully merge) until Region IIc when crystallographic pore growth slows down. The mechanism that results in this cessation in porous layer growth is discussed in our previous work [21]. It is is possibly due to limitations in the ion transport along the pore channels – the effect of which increases as the pores lengthen – or due to a change in electrolyte chemistry because of the accumulation of products from the reaction – the effect of which increases with duration of pore growth. Therefore, after a combination of pore length and time the pores stop growing; *i.e.* the porous layer becomes passivated. If these ion transport limitations did not occur then the increase in potential would result in a further increase in current (Region IIb) as is seen for wafers of higher carrier concentration.

The restricted diffusion of ions in the electrolyte within the pores probably causes saturation of the solution with products from the reaction resulting in precipitation occurring on pore surfaces (Fig. 4γ). The change in the shape of the pore tips at this stage is also visible in this image, with their shape resembling the geometries observed for etching at lower electrolyte concentrations [17]. At higher potentials (Region III and IV in Fig. 3) the current cannot be accounted for by crystallographic pore growth and is due to the non-crystallographic growth mechanisms which occur. It is visible in Fig. 4δ that the non-crystallographic growth, which had just begun in Fig. 4γ, has resulted in the porous layer being under-cut. It follows that this under-cutting corresponds to the shoulder in Region III of the LSV of Fig. 3, while, as has been shown in previous work [13], the rise in current in Region IV corresponds to the formation of a trench around the perimeter of the exposed electrode surface. This continued etching eventually results in a series of current peaks (as shown for the higher carrier concentration sample above 0.43 V in Fig. 5) due to the separation of the porous layer from the substrate until a more planar etching occurs (not shown).

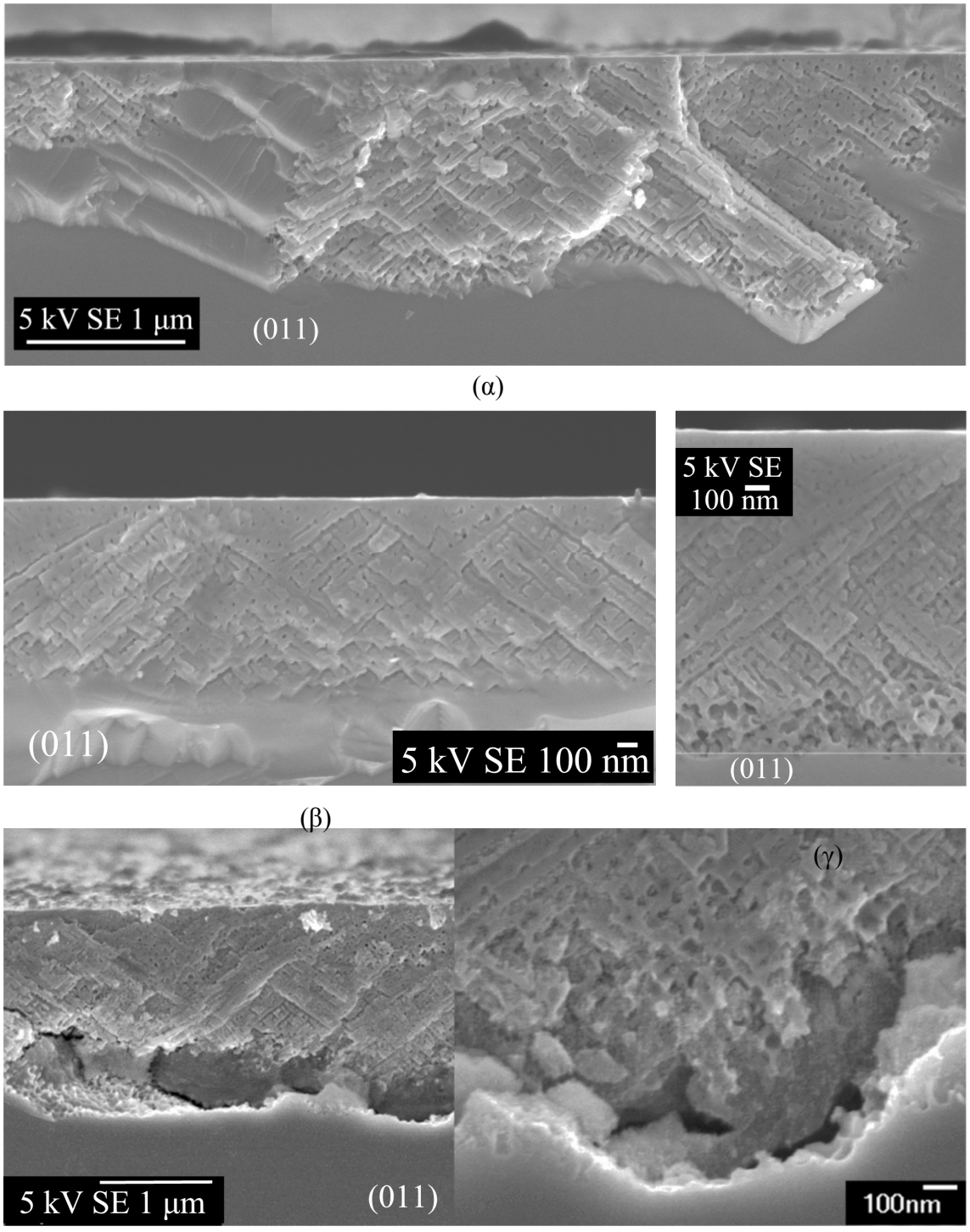


Fig. 4 Cross-sectional SEM micrographs of the (011) cleavage plane of InP electrodes (n = 3.4 x 10^{18} cm^{-3}) after LPSs at 2.5 mV s^{-1} in 5 mol dm^{-3} KOH. Upper potentials of (α) 0.454 V, (β) 0.460 V (peak voltage), (γ) 0.537 V and (δ) 0.730 V corresponding to graph (Fig. 3). Magnified image of porous to bulk interface and oxide precipitates in pores is also shown for (d).

If the carrier concentration of the InP substrate is changed the shape of the LSVs also changes allowing the mechanism to be further investigated. Fig. 5 shows LSVs for three InP samples with carrier concentrations of approximately 3.4 (corresponding to the curve of Fig. 3), 5.3, and 6.7 x 10^{18} cm^{-3}, respectively. It can be observed that the three LSVs are very similar in shape but have some notable differences: *e.g.* a shifting of the curves to lower potentials and a decrease in the magnitude of the first peak with increasing carrier concentration; and at higher carrier concentrations there are two current peaks present (E_{p1} and E_{p2}) compared to lower concentrations where there is only one peak ($E_{p1,2}$).

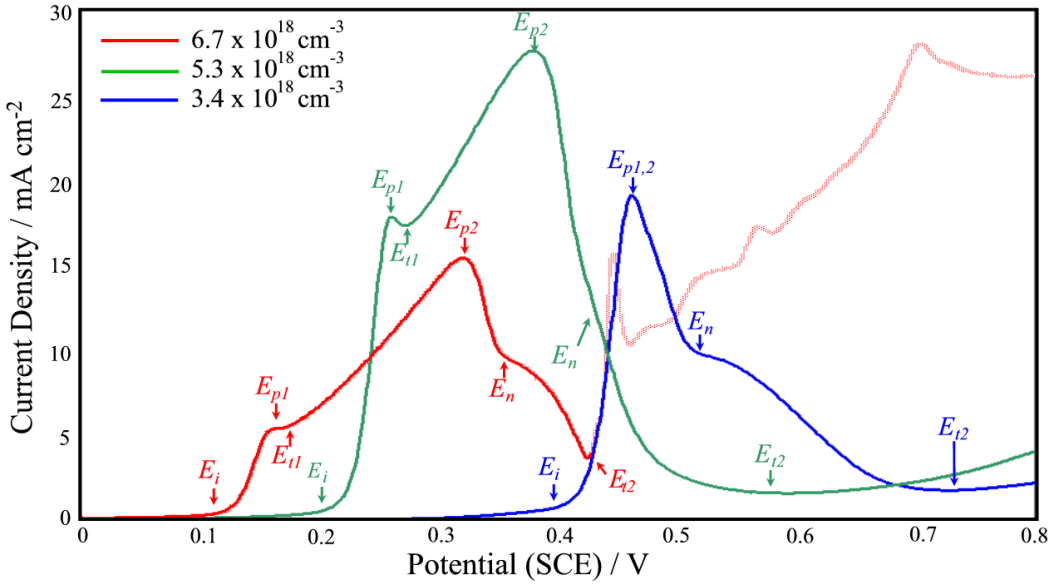


Fig. 5 Linear sweep voltammograms for InP of three different carrier concentrations, n = 3.4, 5 to 5.6 and 6.7 x 10^{18} cm^{-3}, etched in 5 mol dm^{-3} KOH from 0 to 0.8 V (SCE) at 2.5 mV s^{-1}. For the sake of comparison and clarity the peaks that occur after 0.43 V for the highest carrier concentration sample are plotted in a lighter colour.

Pit Initiation and Domain Expansion (*Region IIa*)

Progressive Pit Initiation

Fig. 1a shows the distribution of surface pits after an extended period of etching. Since the micrograph records information from a thin layer just beneath the surface, and not just from the surface, both the pits and the porous structures connected to them are visible. If a sample which has been anodised for a short period of time (*i.e.*, to between E_i and E_{p1} of Fig. 3) is then chemically etched in a H_2SO_4 solution, all the porous structures including the internal skeletons of the domains can be removed [22] as shown in Fig. 6.

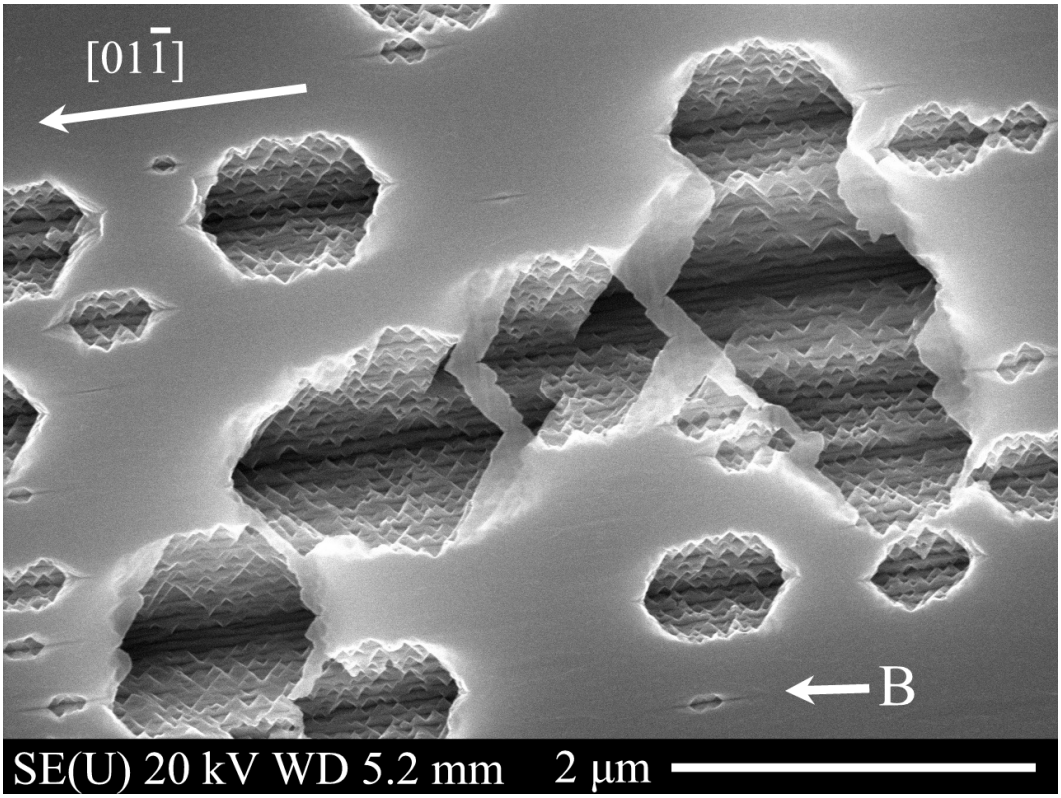


Fig. 6 SEM micrograph of (100) surface InP (n = 3.4 x 10^{18} cm^{-3}) after LPS from 0 to 0.46 V (SCE) at 2.5 mV s^{-1} in 5 mol dm^{-3} KOH. Following the LPS the sample was etched in a heated solution (70°C) of H_2SO_4 for 150 seconds so as to reveal the degree of porous etching.

In this figure the domains were chemically etched by 7.5 mol dm^{-3} H_2SO_4. This method of viewing the domains is destructive but allows an overview of the porous domain progression to be extrapolated. It can be seen that the voids that were once occupied by the truncated tetrahedral domains vary in size. Therefore the assumption can be made that the domains have grown for different periods of time. It can also be seen from the smaller voids (*e.g.*, at B) that only the pores whose projections are along the <01$\bar{1}$> directions grow from the pit first corresponding to the growth of primary pores along the <111>A directions. The elongation of the voids in the <01$\bar{1}$> directions due to the truncated tetrahedral shape can also be seen in the micrograph.

Asymmetry in the Distribution of Surface Pits

The average pit separations observed in SEM figures similar to Fig. 1a are plotted against potential in Fig. 7 and a corresponding LSV is shown for reference. The pit separation was estimated from SEM images with the separation of pits along the [01$\bar{1}$] and [011] axes estimated separately. This was done as follows: The region surrounding each pit was

divided into four triangular quadrants (as shown in the inset of Fig. 7) each of which contained a <011> direction along its central axis. Then in each of these quadrants the shortest component along the central <011> direction of that quadrant (*e.g.* s_v for $[01\bar{1}]$ and s_h for [011]) to a pit was measured. The separation between pits approaches its minimum in the vicinity of potentials near the first peak and the first trough in current.

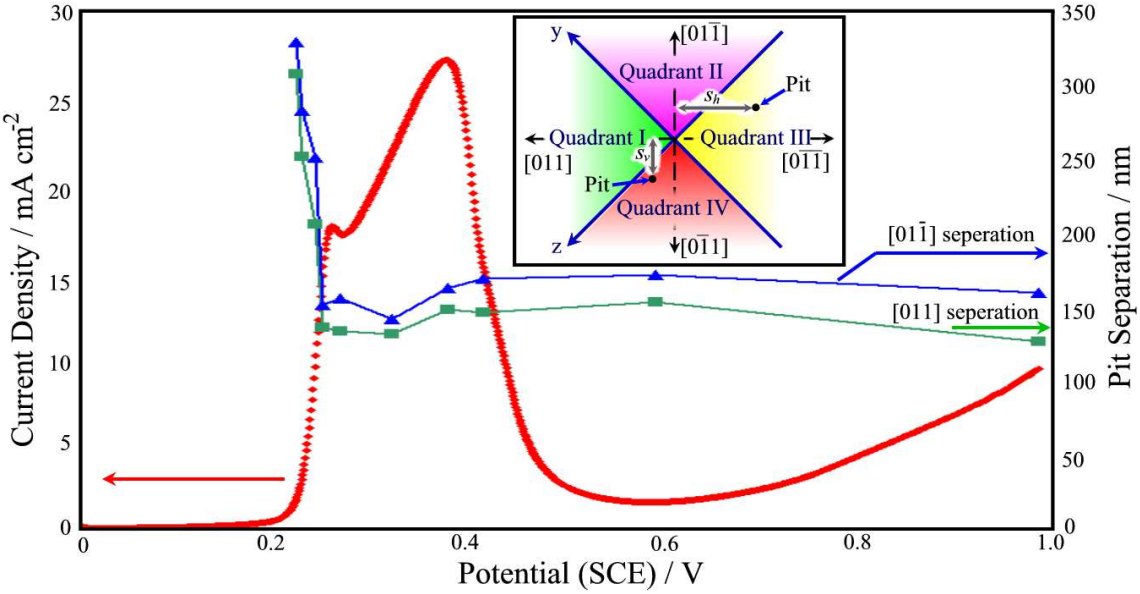


Fig. 7 Linear sweep voltammogram and surface pit separation versus voltage for InP (n = 5 to 5.6 x 10^{18} cm^{-3}) from 0 to 1.0 V (SCE) at 2.5 mV s^{-1} in 5 mol dm^{-3} KOH. Inset: Diagram showing how the regions of the SEM image around a surface-pit were divided into four quadrants along the four <011> directions, allowing the component of pit separation in each <011> direction to be measured.

Interestingly, it is observed in Fig. 7 that there is a small but consistent difference between the separation of the pits along the $[01\bar{1}]$ axis and the orthogonal [011] axis (despite the variations inherent in the data due error caused by the complexity of the measurement system) with the former value always being slightly larger than the latter. Initially, between 0.225 and 0.23 V, this ratio is ~1.1 with average $[01\bar{1}]$- and [011]-separations of 350 nm and 320 nm, respectively, but it then increases slightly to ~1.15 as the average pit separations decrease to 184 nm and 160 nm, respectively. Presumably, this slight asymmetry is due to the domain shape and the growth of the initial two pores along the $[01\bar{1}]$ axis (as shown at B in Fig. 6).

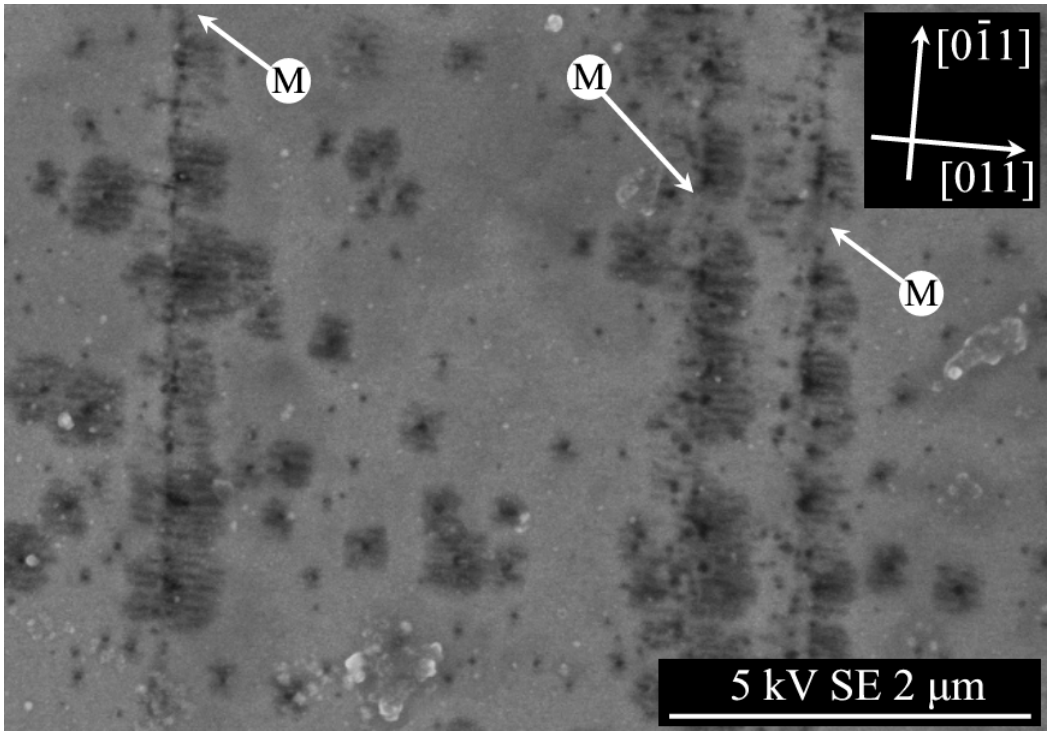


Fig. 8 SEM (100) surface image of InP (n = 5 to 5.6 x 10^{18} cm^{-3}) containing porous domains that have been etched in 7.5 mol dm^{-3} H_2SO_4 for 90 s at 70°C. The larger domains can be seen to originate along three scratch lines shown in the image. The domains were formed by a linear potential sweep from 0 to 0.245 V (SCE) at 2.5 mV s^{-1} in 5 mol dm^{-3} KOH.

Pit Location with Respect to Scratches (Physical Defects)

Fig. 8 shows another SEM surface image of an InP sample after an LPS to a potential prior to the first anodic peak but with the surface of the sample deliberately scratched by tweezers (at M) prior to anodisation. This was done so as to investigate the effect of surface defects. After the anodisation and prior to viewing the sample in the SEM the porous structures were chemically etched (in 7.5 mol dm^{-3} H_2SO_4 for 90 s at 70°C) so as to increase the visibility of the sub-surface structures but without causing any over etching as seen in the previous image so that the scratches would still be visible. As can be observed both surface and sub-surface features are visible allowing the surface pits belonging to young (small) and more mature (large) domains to be distinguished. It can be observed that the larger domains – which would have formed first – are located along the scratch lines and a lower density and smaller average domain size occurs elsewhere. This distribution could be due to a combination of factors caused by the scratch marks; The scratches would have increased the local surface curvature, formed screw defects, and exposed {111}B surfaces. Increased curvature along the scratches would increase electric field and therefore increase quantum tunnelling while

the exposure of {111}B phosphorous atoms could facilitate etching and the initiation of pit formation. Previous work by Schmuki *et al.* [23] showed similar behaviour for anodisation in HCl and attributed the behaviour to changes in the space charge layer geometry near defect sites.

Comparison of Pit Densities and Domain Merging to LSVs (*Region IIa and IIb*)

Fig. 9 shows a LSV in conjunction with the corresponding surface-pit density statistics with both the current density and the surface-pit density plotted against potential. The density of surface pits was recorded by performing LPSs as far as each potential and then examining the surface using SEM. As expected, an inverse of the trend seen for pit separation (*i.e.* Fig. 7) was observed. It can be seen from the LSV that there are two current density peaks, the first at 0.252 V and the second at 0.383 V and that the pit density reaches a maximum value just after the first of these two peaks and near a trough in current at E_{t1}.

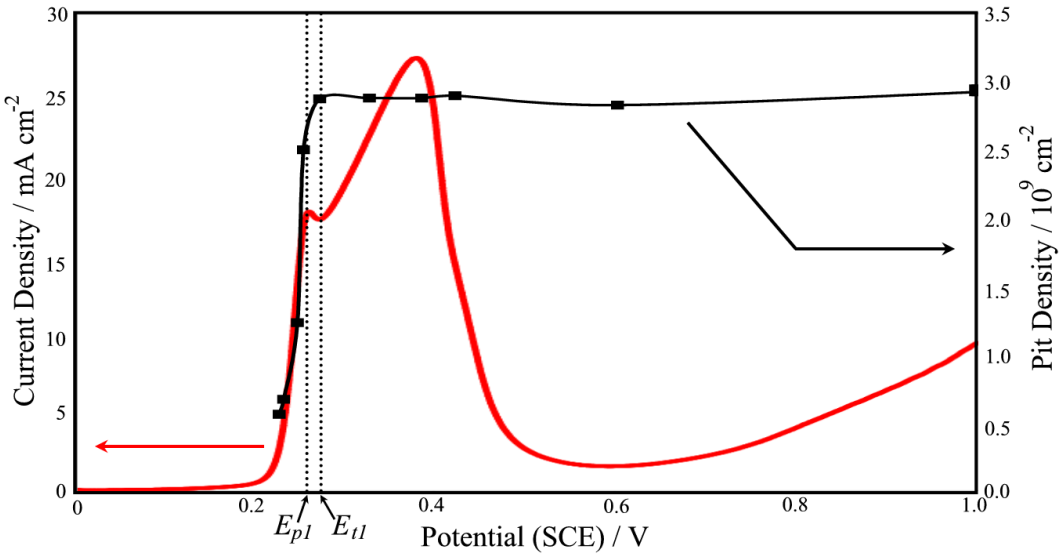


Fig. 9 Linear sweep voltammogram and surface pit density versus voltage for InP (n = 5 to 5.6 x 10^{18} cm^{-3}) from 0 to 1.0 V (SCE) at 2.5 mV s^{-1} in 5 mol dm^{-3} KOH.

Fig. 10 shows an SEM (011) cross-section of a porous layer after a LPS from 0 to 0.27 V (*i.e.* corresponding to E_{t1} in Fig. 9). Several different domains, or pores growing from several different origins, can be observed in this micrograph. Not alone have these domains begun to merge but they have merged fully so as to form a continuous layer with no remaining regions of dense InP isolated from the bulk InP (between domains and within the porous layer).

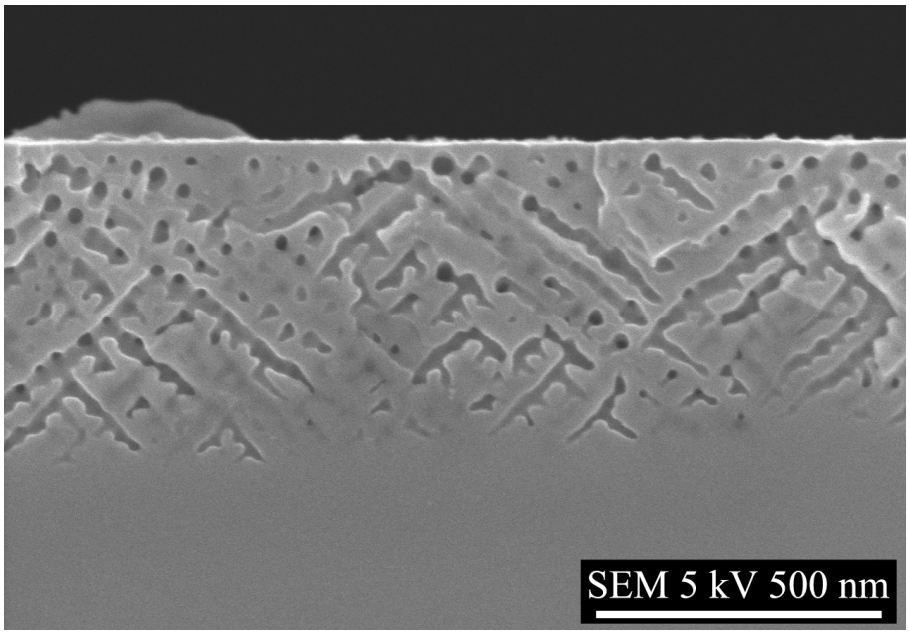


Fig. 10 SEM micrograph of (011) cleavage plane following a LPS from 0.0 to 0.27 V (SCE) (small trough after 1st current peak) (n = 5 to 5.6 x 10^{18} cm^{-3}) showing the cross-sections of young porous domains that have merged fully into one continuous layer.

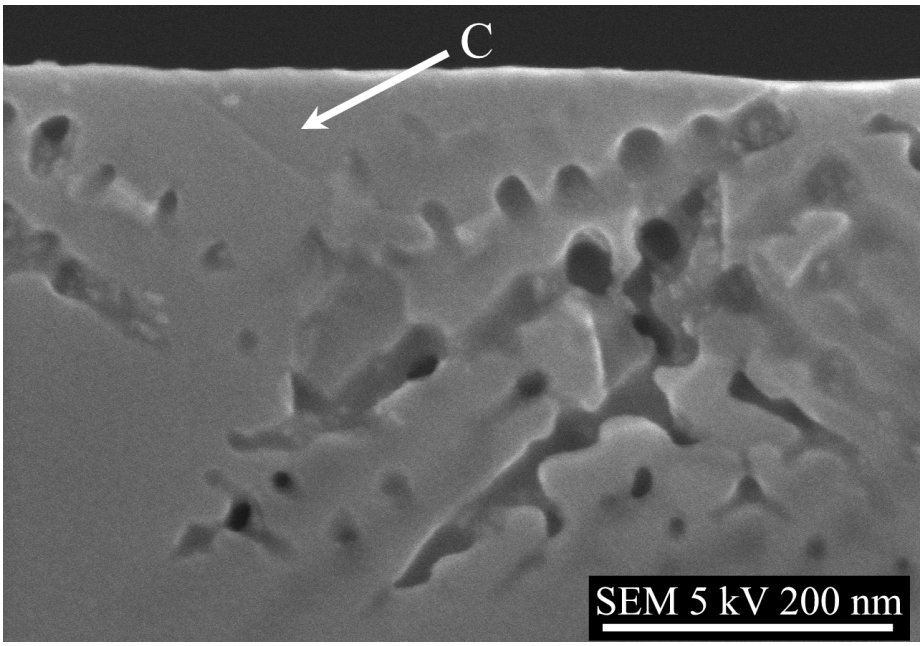


Fig. 11 SEM micrograph of (011) cleavage plane following a LPS from 0.0 to 0.252 V (SCE) (1st current peak) (n = 5 to 5.6 x 10^{18} cm^{-3}) showing the cross-sections of young porous domains that have begun to merge but have not completed the process since there is a non-porous region visible at C.

Fig. 11 shows an SEM (011) cross-section of a porous layer after a LPS from 0 to 0.252 V (E_{p1} in Fig. 9). Two partial domain cross-sections can be observed in this image. It can be seen that merging of domains has just started at this slightly earlier stage of the experiment. However, as can be seen at C in Fig. 11, some of the regions between the merging domains are not porous since the porous domains have not merged fully.

Fig. 12 shows an SEM (011) cross-section of a porous layer after a LPS from 0 to 0.245 V, corresponding to just before the first current peak at E_{p1} in Fig. 9. Unlike the two previous images merging of domains has not begun and three isolated domain cross-sections, along with their surface-pits can be seen in the image. It follows from this analysis of cross-sectional SEMs that prior to E_{p1} isolated domains exist while after this at E_{t1} all the domains are merged into one continuous porous layer. It is therefore very likely that the first current peak is caused by the merging of domains and that the decrease in current is due to the decrease in the number of active pore tips as the merging process is completed between E_{p1} and E_{t1}.

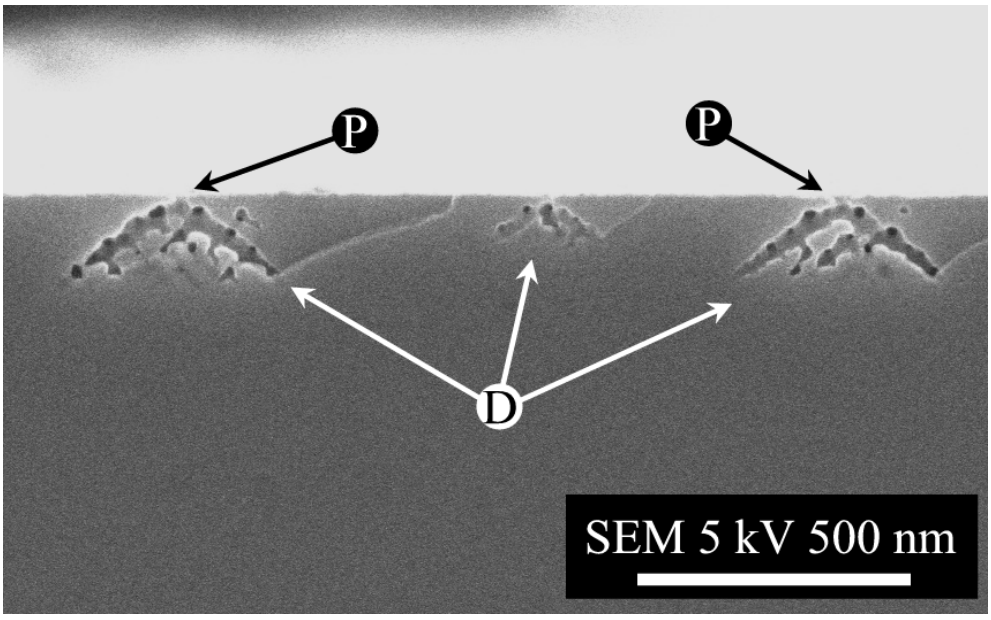


Fig. 12 SEM micrograph of (011) cleavage plane following a LPS from 0.0 to 0.245 V (SCE) (just before 1st current peak) (n = 5 to 5.6 x 10^{18} cm^{-3}) showing the cross-sections of young porous domains, which have not begun to merge.

At the same time as the merging of domains is completed the surface pit density saturates as shown in Fig. 9. In this figure it can be seen that the pit density saturates near E_{t1} and not at E_{p1}. This is as expected since the formation of pits is dependent on the availability

of carriers that can tunnel across the depleted region that forms a near-surface layer of non-porous InP (which is depleted of carriers during anodisation). Therefore as the domains begin to merge together this near-surface layer can only be etched in the regions where there is no porous structure beneath the electrodes surface: *i.e.* where the domains have not merged fully. However, until merging has completed (at E_{t1}), there is still bulk InP just beneath the surface and therefore pits can still form resulting in pit saturation not occur until merging of the domains is completed at E_{t1}. Furthermore, since the increase in pit density corresponds with the increase in current density, it can be concluded that the first current increase and peak is as a result of both the increase and saturation of pit density, and the expansion and merging of domains into a continuous porous-layer. In addition, the trough in current can be associated with a decrease in the number of active tips and a reduction in new pit formation (surface etching) to virtually zero.

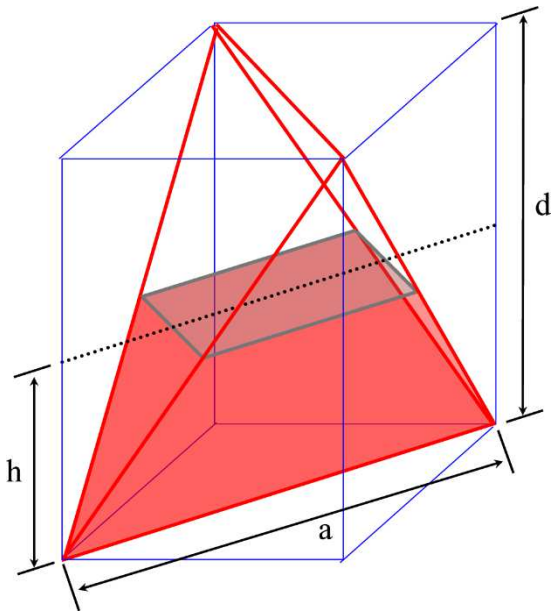


Fig. 13 Tetrahedron enclosed by a cube of side d. The lower half of the tetrahedron represents the overall volume of an individual porous domain.

Model of Domain Merging

The charge required to grow a continuous porous layer can be calculated from SEM and LSV data. Therefore, if the domain shape of the pores growing from an individual surface pit is presumed to be a truncated tetrahedron, it is possible to calculate the current required to form such a domain of pores. In such a model the electrode-surface area can be divided into a matrix of rectangular regions with one pit per region allowing the current density of such a region to be calculated by dividing the pit current (i_{pit}) by the area of the region (A_D). A

mathematical model can be formulated if it is assumed (for the sake of the model) that the matrix is regular with each of its regions being equal in size and shape. The pit that forms in the centre of each region can be assumed for simplicity to form at the one time as all other pits in all the other regions. It follows therefore that the current density of one of these regions is equivalent to the current density for the overall surface. Of course, as explained earlier it is not valid to assume that pits are homogenously distributed and that they all initiate at the same time and therefore the results of this mathematical model will only be approximate.

Fig. 13 shows a schematic of a tetrahedron with the lower half of the tetrahedron corresponding to the tetrahedral domain shape form in InP. [10] From this figure the volume of the lower truncated tetrahedron, V_D, can be calculated.

$$V_D = \frac{d^3}{6} \qquad [1]$$

where d is the length of the side of the cube of which four of its corners correspond to the four vertices of the overall (non-truncated) tetrahedron. Since charge, Q_D, is proportional to the etched volume, V_D, the current, i_{pit}, must be proportional to the derivative of volume with respect to time:

$$Q_D = \frac{nFP}{V_{M,InP}} \times V_D \qquad [2]$$

$$\Rightarrow i_{pit} = \frac{d(Q_D)}{dt} = \frac{nFP}{V_{M,InP}} \times \frac{d(V_D)}{dt} \qquad [3]$$

where $V_{M,InP}$ is the molar volume of InP, P is the porosity of the porous structure formed, n is the number of electrons per formula unit of InP and F is the Faraday constant.

By dividing Q_D and i_{pit} by A_D both the charge density, q, and current density, j, for the overall electrode surface can be approximated:

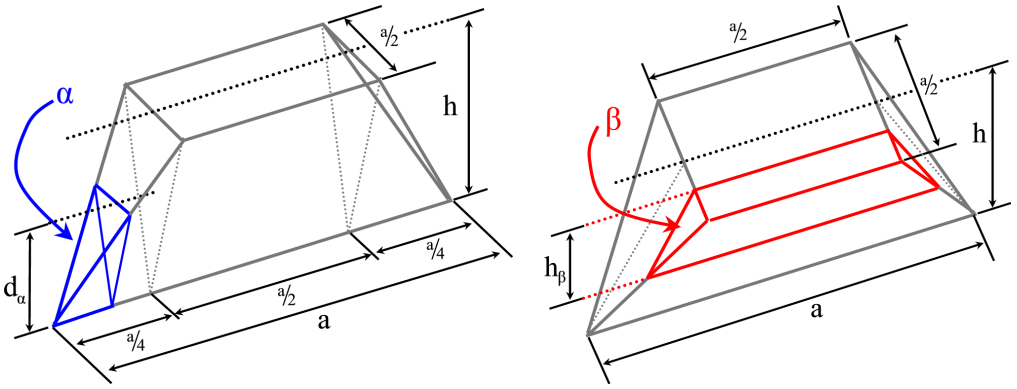
$$q = \frac{nFP}{V_{M,InP}} \times V_D \qquad [4]$$

$$j = \frac{nFP}{A_D V_{M,InP}} \times \frac{d(V_D)}{dt} \qquad [5]$$

When domains merge together and the expansion of V_D is restricted so that it no longer expands at the same rate. The volumes of the regions where a domain can no longer expand into (but would have if it were an isolated domain) can be calculated from Fig. 14:

$$\alpha = \frac{1}{6} d_\alpha^3 \quad \text{and} \quad \beta = \frac{1}{6} h_\beta^3 + \frac{1}{2} h_\beta^2 h \qquad [6]$$

where α and β represent the volumes that the merging domain cannot grow into along the $[01\bar{1}]$ and [011] directions, respectively. Adjusting the domain volume for these should allow the approximation of how the current should behave as a result of domain merging.



(a) (b)

Fig. 14 Schematics are shown of isolated domains of depth h. (a) The region marked α represents the volume the domain was unable to expand into due to merging with another domain along the $[01\bar{1}]$ direction (b) while the region marked β represents the volume the domain was unable to expand into due to merging with another domain along the [011] direction.

Eventually these regions α and β overlap each other and extend outside of the electrode surface. When this happens adjustments must be made to α and β (as shown in the appendix) so as to calculate the correct V_D. Once these adjustments are made the domain volume V_D can be calculated during merging and from this both the charge density, q, and current density, j, can be calculated for an electrode during domain merging from

$$V_D = \frac{d^3}{6} - \sum\alpha - \sum\beta \qquad [1^*]$$

where Σα represents the reduction in volume due to merging along the $[01\bar{1}]$ and $[0\bar{1}1]$ directions and Σβ represents the reduction in volume due to merging along the [011] and $[0\bar{1}\bar{1}]$ directions.

Comparison of Model to Experiment

Fig. 15 shows a plot of current density versus time for a potential-step experiment where the potential is held at 0.3 V (SCE) and for a linear sweep experiment where the potential is

scanned positively from 0 V (SCE) at 2.5 mV s^{-1}. Plots for the current density, *j*, calculated by the domain merging model are also plotted on the same graph. In the model it was presumed (from SEM images of continuous porous layers as shown later) that the porosity of the grown layers was 21% while the parameters of initiation potential, pit separation and layer-deepening rate were used as varible parameters.

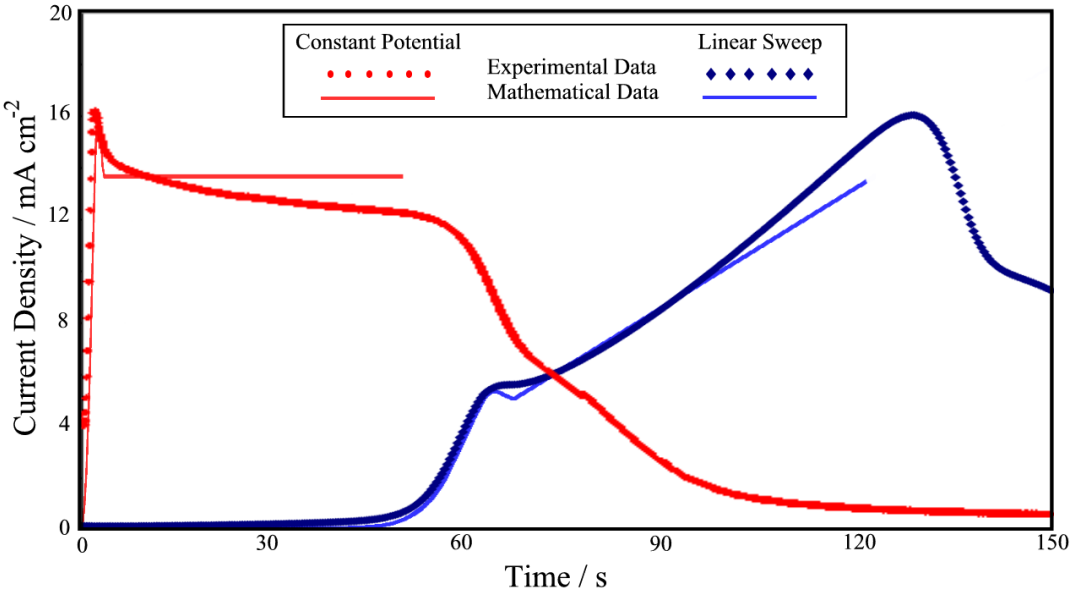


Fig. 15 Plot of the numerically-calculated (▬/▬) and from-experiment (●/◆) current-density data for both a potential-step experiment, at a potential of 0.3 V (SCE) (▬/●), and for a linear sweep experiment, at a potential sweep rate of 2.5 mV s^{-1} (▬/◆). The experimentally samples were from the same n-InP wafer ($n \approx 6.7 \times 10^{18}$ cm^{-3}). For the mathematical model a porosity of 21%, a linear increase in the rate of porous layer deepening along the [$\bar{1}$00] direction from 0 nm s^{-1} at 0.09 V to 25 nm s^{-1} at 0.3 V were used. In the potential-step model surface-pit separation along the [011] and [01$\bar{1}$] directions were 126 nm and 90 nm, respectively, while in the case of the linear-sweep model they were 210 nm and 150 nm, respectively,

In both the potential-step model and experiment the current does not reach its maximum value immediately but instead takes several seconds. This similarity is continued after this maximum value since the current falls off to a plateau in current. Experimentally the fall off is less rapid. This difference may be because experimentally there is a distribution of pit spacing and pits do not form at exactly the same time. Consequently, domains do not merge simultaneously as they do in the model. Indeed, in experimental results there is a slight variation in the position of this peak between experiments carried out under the same

conditions even if the samples are cleaved from the same wafer. It follows that the current peak in the model decreases faster than experimental results show. Experimentally, the plateau region is not exactly horizontal and there is an eventual decrease in current from this plateau; the non-zero slope in the plateau region and the eventual fall-off in current are presumably due to an initial slow-down in the layer growth-rate followed by a change in etching mechanism (*i.e.* the cessation of crystallographic oriented porous layer growth). Since the numerical model assumes a constant etching rate at the pore tips (for a constant applied potential), the gradual decrease in current and the eventual fall-off does not occur in the model.

The model was also used to model the current for a linear increase in potential, as shown in Fig. 15. In the model it was assumed that after a threshold/initiation potential there was linear increase in the rate of pore tip progression so that the rate at 0.3 V is the same as in the 0.3-V potential-step model. Therefore, the data was scaled through variation of the parameters of initiation-potential and pit-separation. As in the previous case there is a difference between the model and experiment but the model and the experimental results are seen to be in close agreement. After the first peak in current the model displays a greater fall-off in current, presumably due to the domains not all merging at the same time. Unlike the potential-step experiment, which shows a decrease in the current relative to the plateau region of the model, the linear region in the model after the peak shows currents that are less than the experimental values with the experimental values for current increasing more rapidly. This means that experimentally the etch-rate increase at the pore tip must be more rapid than a proportional increase with respect to applied potential. After the linear region the similarities between experiment and model are lost, as in the potential-step case, possibly due to a change in mechanism which results in a fall-off in current after the second peak in the experiment.

It can be concluded from the mathematical model that the domain shape has a significant effect on the current density in potential-step experiments and linear sweep voltammetry resulting in the formation of the first current peak associated with domain merging and a plateau/linear region associated with the widening of the continuous porous layer. This is in agreement with the earlier SEM observations where domain merging coincides with the first anodic LSV peak and trough. It follows that a source of the current

peak both in potential-step experiments and in LSVs results from merging of truncated tetrahedral domains.

Growth of the Continuous Porous Layer (Region IIb)

Comparison of Layer Thicknesses and Porosity to LSVs

Fig. 16 shows the same LSV that was shown previously in Fig. 7 but this time the average layer thickness measured from the bottom of the near-surface layer to the lower edge of the porous layer/domain is also plotted against potential. It can be seen in this graph that once pore formation starts the layer thickness gradually increases to a maximum thickness of almost three microns. This saturation point occurs after both peaks in current and coincides with an inflection point on the LSV at 0.42 V; *i.e.* after this inflection point the porous layer does not etch any deeper into the substrate and measurements of layer thickness are the same and independent of potential and time for the remainder of the experiment.

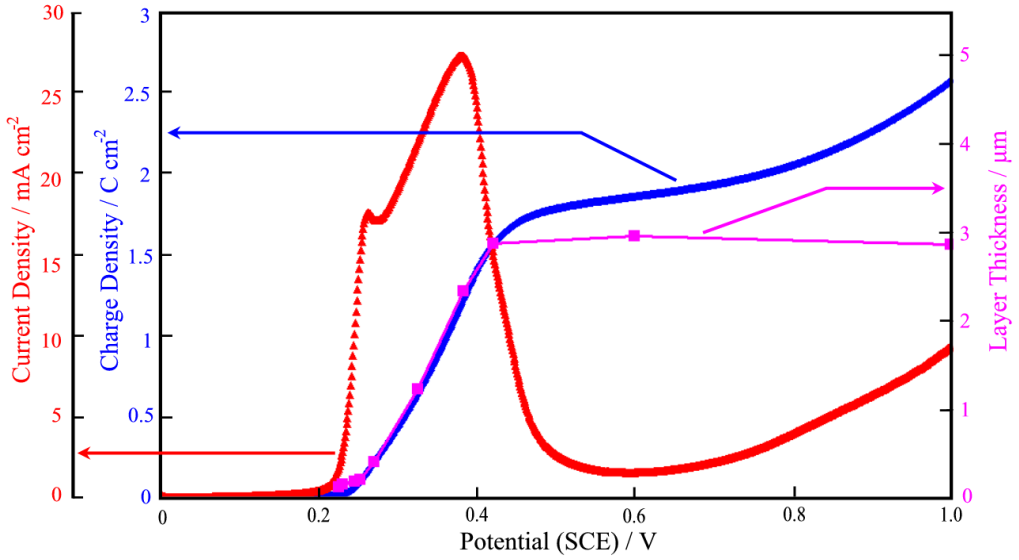


Fig. 16 Linear sweep voltammogram and SEM (011) porous layer thickness measurements versus voltage for InP (n = 5 to 5.6 x 10^{18} cm^{-3}) from 0 to 1.0 V (SCE) at 2.5 mV s^{-1} in 5 mol dm^{-3} KOH. Charge passed and SEM (011) porous layer thickness measured versus potential for a linear potential sweep of InP (n = 5 to 5.6 x 10^{18} cm^{-3}) from 0 to 1.0 V (SCE) at 2.5 mV s^{-1} in 5 mol dm^{-3} KOH.

Fig. 16 also compares the layer thickness data and the graph of charge consumed during etching against potential. It can be seen that until the inflection point the layer thickness is proportional to the charge passed, except during the initial rise in current where there is a

slight mismatch between the two curves, suggesting that the porosity is constant during the region where the curves overlap. Since the charge passed is a measure of the amount of material etched, Faraday's law allows the (coulometric) thickness d_c of a compact InP layer, which is equivalent to the quantity of InP etched by charge Q, to be calculated by the equation

$$d_c = \frac{Q}{S}\frac{V_{M,InP}}{nF} \qquad [7]$$

where S is the surface area of the electrode, $V_{M,InP}$ is the molar volume of InP, n is the number of electrons per formula unit of InP and F is the Faraday constant. Using a value of 30.31 $cm^3\ mol^{-1}$ for $V_{M,InP}$ [24] and assuming n = 8, values for d_c were calculated.

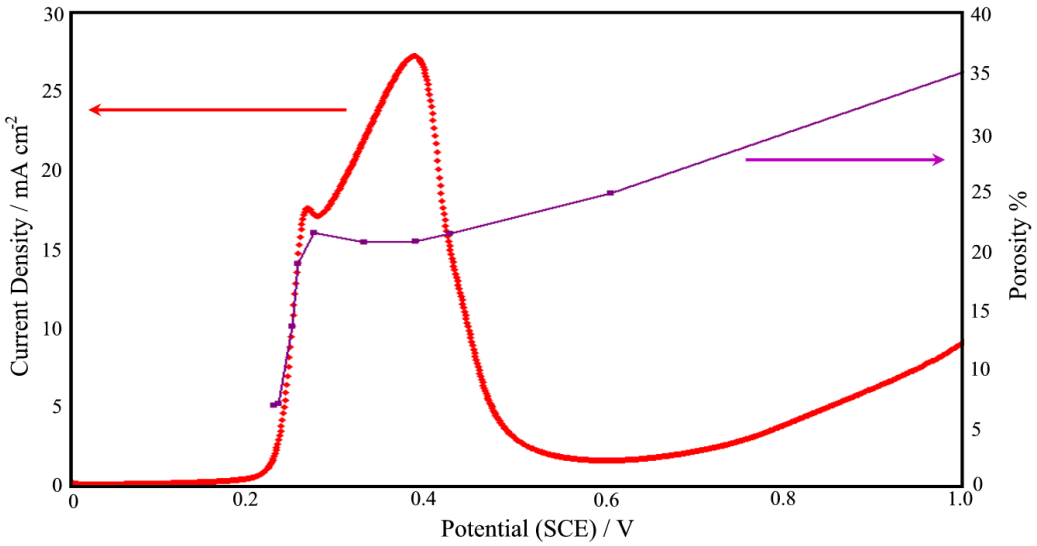


Fig. 17 Linear sweep voltammogram and apparent layer porosity versus voltage for InP (n = 5 to 5.6 x 10^{18} cm^{-3}) from 0 to 1.0 V (SCE) at 2.5 mV s^{-1} in 5 mol dm^{-3} KOH.

Since the porosity p is the ratio of the thickness d_c, which represents the quantity of InP removed, to the corresponding as-measured porous-layer-thickness d_e, the porosity

$$p = \frac{d_c}{d_e} \qquad [8]$$

determined from the values of d_e and d_c can plotted against potential as shown in Fig. 17. The LSV corresponding to the porosity data is also plotted on this figure so as to allow comparisons to be made. Prior to the first current peak the measurements of d_e are of domain depths rather than layer thicknesses and as these domains widen to form a continuous layer the corresponding porosity of the uniform layer that the domains form increases until it

saturates at ~21%. It can be seen from the graph that this saturation occurs close to the trough in current verifying that domain merging is fully accomplished at this potential/time in LPSs. During the apparent linear region of the LPS – between the current through and the second current peak – and as far as the inflection point after the second peak the level of porosity stays approximately constant. This temporary invariance is expected, since deepening of a uniform layer is observed by SEM images in this region and pore width is constant at ~28 nm throughout, verifying the assumption that was made (in the mathematical model) that electrochemical etching is occurring only in the vicinity of pore tips and not within the porous layer at the pore walls. At potentials greater than the potential of the inflection point in the LSV – corresponding to the saturation of porous layer thickness – the experimental thickness of the layer (d_e) stays constant while the coulometric thickness (d_c) continues to rise resulting in an overall increase in the porosity curve (*i.e.* the thickness and charge plots in Fig. 16 are observed to diverge). This increase in porosity corresponds to the cessation of <111>A-pore-growth etching; *i.e.* the saturation of porous layer thickness; and the commencement of non-crystallographic etching mechanisms.

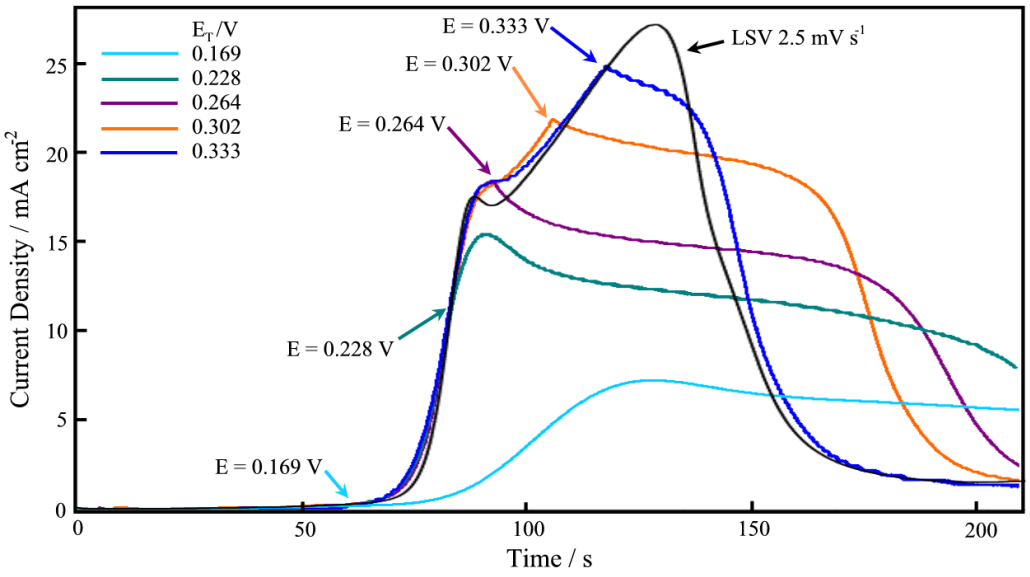


Fig. 18 Graph of current density plotted against time for InP samples (n = 5 to 5.6 x 10^{18} cm^{-3}) anodized by a linear potential sweep at 2.5 mV s^{-1} in 5 mol dm^{-3} KOH from 0 V (SCE) to a plateau potential, E_T. Once E_T was reached each experiment was held at the plateau potential. An LSV is also plotted on the same axes for comparison purposes.

Dependence of current on change in potential and time during a LPS

More in-depth analysis of the behaviour of the LPSs can be performed by conducting several 'potential- ramp experiments' so as to investigate the dependence of the current on time and potential. That is a LPS is run as far as the potential of interest, E_M, and then the potential is held constant at E_M for the remainder of the experiment. It follows that if for $E > E_M$ the current in an LPS normally increases but where E is held constant at E_M the current increases at almost the same rate, then the process must be largely time dependent. However, if the current changes from increasing to being constant or decreasing it can be concluded that the increase in current after E_M in the LSV was mainly due to the change in potential.

A set of curves using this technique is shown in Fig. 18. It is apparent in this graph that stopping the increase in potential prior to the first peak at 0.264 V causes a decrease in the rate of current increase but the current still continues to increase. Therefore, prior to the first peak, the current is dependent mainly on time and not just potential. This is different to the response after the first current peak suggesting that the linear increase in current between the two current peaks is mainly dependent on potential.

In experiments where E_M is held at 0.302 V (in Fig. 18), an almost constant current results indicating that the process has reached a quasi steady-state and therefore indicates that the current at E_M on the LSV is almost independent of time and dependent on potential. Such behaviour is as expected since SEM micrographs show the thickening of a continuous porous layer of constant porosity as shown in Fig. 17 (which should cause little change in the number of active pore tips). However there is a slight decay that is gradual and linear (*e.g.* between 120 and 170 s). Therefore, within the mechanism at constant potential there is an almost linear decrease in the etch-rate at the pore tip and in the LSV the current in this region can be said to have a large positive dependence on potential but also a slight negative dependence on time.

While the concept of current having a dependence on potential is easy to grasp it is much harder to comprehend the dependence of current on time. Indeed, along with the dependence due to the growth and merging of domains (as is the case for the 1st anodic peak), there are other time effects. Such effects could result from the lengthening of pore channels, the change in electrolyte composition or the variation of tip shape with time. As a pore channel lengthens an increase in the ohmic resistance occurs along the channel resulting in a decrease in tip potential. If a change in electrolyte composition occurs with time it could

cause changes in electrochemistry at the semiconductor-electrolyte interface which could have direct effects on etch rate or indirect effects through alteration of the tip shape. The tip shape can also be altered by several factors: time, growth rate, propagation direction and proximity of other pores. Such changes in electrolyte chemistry and potential at the pore tip could result in the tip loosing its sharpness and therefore could lead to the termination of etching at the tip due to a decrease in the electric field at each tip.

Tip propagation, electrolyte flow and species diffusion

Since the current is almost linear after the first peak in LSVs it follows that both the average propagation speed and rate of increase in speed of the continuous porous layer widening can be calculated from this linear region to be 43 nm s^{-1} and 0.4 nm s^{-2} (or 0.16 nm s^{-1} mV^{-1} for a scan rate of 2.5 mV s^{-1}), respectively. Therefore if the pores are growing along the <111>A directions this would correspond to an etch rate at the pore tips of 74 nm s^{-1} and an acceleration as the potential is scanned at 2.5 mV $s^{-1}$of 0.7 nm s^{-2} (or 0.28 nm s^{-1} mV^{-1}) at 0.3 V (*i.e.* half way between the two current peaks).

The average current per pit can be calculated by dividing the current density by the density of surface pits. The resulting current per pit at either of the two current peaks is approximately the same value (~8 pA). To give an idea of how significant a current this is it is important to remember that for a typical domain all of this current must flow a pit of diameter 17 nm (on average). Therefore, the pit current density, j_{pit}, can be calculated and is found to be ~3.8 A cm^{-2} at the either of peaks in current. This is a very high current and emphasizes the large flow of charge through each surface pit. Along with the flow of charge there is also a flow of materials (reactants, products and supporting electrolyte) due to the movement of charge but also due both to concentration differences and pressure differences – caused by the volume change of materials as they change from reactants to products.

While the flux of different materials due to diffusion caused by the concentration differences are dependent on the structure of the porous network the flow through the pit opening resulting from volume changes as the reactants react to form the reaction products is independent of the network's structure and can therefore be estimated from the current flowing through a typical pit.

As mentioned in previous work [12] we assume the following eight electron reaction to take place at the pore tip:

$$InP + 8OH^- + 8h^+ \rightarrow In^{3+} + PO_4^{3-} + 4H_2O \quad [9]$$

The products of this reaction can result in a number of different combinations of inorganic compounds, *e.g.* $InPO_4 + 4H_2O$, $½In_2O_3 + ½P_2O_5 + 4H_2O$ and $In(OH)_3 + H_3PO_4 + H_2O$. Using these examples the volume of the reactants and products can be approximated. It follows that there may be a decrease in volume as a result of the reaction at the tips with the products occupying a smaller volume than the reactants. Therefore, as InP is etched electrolyte may need to flow into the porous structure. It follows that, while crystallographic pore growth is occurring, a significant fraction of the reaction products may be contained within the electrolyte of the porous structure. If this is the case the chemistry of the solution within the pores must be greatly changed from that of the bulk electrolyte and may be the main reason for the cessation in porous-layer widening.

Therefore, in summary, the LSV can be broken up into the following regions:

I. Where prior to E_i no significant etching occurs.

IIa. After E_i is reached, surface pits form that become the origin of <111>A crystallographic pores. These pores form domains from each pit which expand until just before E_{p1} and then merge into a continuous layer by E_{t1}.

IIb. After a continuous layer has formed the layer continues to deepen between E_{t1} and E_{p2}.

IIc. At an extended period of etching the crystallographic pore growth process slows causing a decrease in current between E_{p2} and E_n.

III. An arrest in the fall-off of current occurs at E_n due to the onset of non-crystallographic etching at the interface of the porous layer and the bulk substrate; (until E_{t2}) this etching leads to widening of the pores near this interface and formation of caverns that undercut the porous layer. In LSV this non-crystallographic pore growth is observed as a shoulder in the current but eventually the current continues to decrease possibly due to changes in the chemistry of the electrolyte in the porous layer.

IV. Above E_{t2} etching of a perimeter-trench causes an increase in current and eventually (along with the under-cutting of the porous layer) leads to the separation of the porous layer from the substrate and the onset of a more planar mechanism of etching (which is not discussed in this paper).

CONCLUSIONS

Examination of the development of surface pits, sub-surface porous layers and other features resulting from the anodisation of (100) n-InP in 5 mol dm^{-3} KOH was carried out using LSV, SEM and mathematical modelling. These experiments showed that saturation in the number of surface pits coincides with the merging of porous domains into a continuous porous layer beneath the electrode surface and the appearance of anodic peaks in current during LSV. Each surface pit acts as the nucleus for the formation of truncated tetrahedral domains beneath a near-surface layer of dense InP. An initial increase in current density occurs in LSVs when a potential is greater than the pit formation potential is reached. This increase results from domain expansion and the formation of new pits in the surface – both of which result in an increase in the number of active pore-tips. Mathematical modelling of this process shows - with support from SEM images - that as these domains merge together to form a continuous porous-layer, the slight fall in current after the peak occurs in LSV and potential-step experiments due to the reduction in the number of active pore-tips to a steady-state value.

Once this continuous porous layer has formed, the number of pore tips stays constant. Therefore for constant potential experiments an almost horizontal region occurs after the anodic peak. In such experiments a small time-dependent decrease in the current is attributed to a decrease in the etch rate at the pore tip due to a change in tip chemistry and/or a decrease in potential at the tip as pores increase in length and/or products build up along the pore channels. In the case of LPSs the increase in potential with time after the first peak in current results in a potential-dependent increase in the current density that compensates for the time-dependent decrease. For some carrier concentrations this increase appears as a region of linear increase in current density and corresponds to an increase in the thickness of the porous layer and in the rate of progression of the active pore-tips. In general carrier concentration has a significant effect on the pore growth mechanism shifting the position of peaks and even their order but does not change the underlying processes that take place with all experiments exhibiting a termination in crystallographic growth after an extended period of etching leading to a sudden fall-off in current after the potential dependent rise in current in LSV experiments and the plateau region of potential-step experiments. After this fall-off in current SEM images show the presence of some degree of non-crystallographic etching in all experiments which is displayed as a shoulder in plots of current vs time. This non-crystallographic etching has the same appearance as etching observed in low concentration

solutions suggesting - along with the presence of precipitates, both within the pore channels and on the electrode surface - that it is the change in chemistry at the pore tip that results the etching mechanism changing from <111>A-crystallographic to non-crystallographic etching.

Estimation of the flow of solution and diffusion of products within the pore channels during etching supports that there may be significant accumulation of products within the network of channels at least until crystallographic etching ceases.

Acknowledgements

The authors would like to thank the Irish Research Council for a postgraduate scholarship funding to perform this research.

Appendix

As described in the main text a formula can be calculated for the volume of a truncated tetrahedral domain, V_D, with respect to its depth, h:

$$V_D = \frac{d^3}{6} \qquad [A1]$$

where d is the length of the side of the cube that the tetrahedron is drawn within or $d = 2h$ where h is the depth of the porous layer. When this domain merges with other domains, the volume associated with the surface-pit that this domain grows from can also be represented by a formula taking into account the volumes of the domain that can no longer grow in the $[01\bar{1}]$ and [011] direction (α and β respectively) and subtracting them from the overall volume (see Fig. 14).

$$\alpha = \frac{1}{6}d_\alpha^3 \quad \text{and} \quad \beta = \frac{1}{6}h_\beta^3 + \frac{1}{2}h_\beta^2 h \qquad [A2]$$

From this volume the charge density and current density required during the growth of a porous layer can then be calculated

$$q = \frac{nFP}{A_D V_{M,InP}} \times V_D \qquad [A3]$$

$$j = \frac{nFP}{A_D V_{M,InP}} \times \frac{d(V_D)}{dt} \qquad [A4]$$

respectively, where $V_{M,InP}$ is the molar volume of InP, n is the number of electrons per formula unit of InP, F is the Faraday constant and A_D is the area of the electrode-surface region associated with the domain i.e. the total are of the electrode divided by the number of pits or the product of the separation along the [01$\bar{1}$] and [011] directions ($A_D = s_a \times s_b$).

Along with the corrections of α and β to the domain volume V_D it is also necessary to make corrections to α and β. These corrections must be made where the α and β volumes overlap each other or extend past the electrode surface. Figure A1 shows a situation where α extends past the electrode-surface and therefore must be corrected by a volume X.

$$X = \frac{1}{2}(d_\alpha - h)^2 \left[h + \frac{d_\alpha - h}{3} \right] \qquad [A5]$$

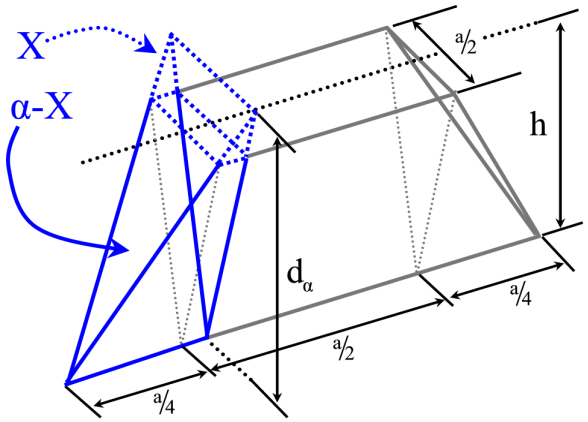


Fig. A1 Schematic of an individual domain of depth h where the region marked α (representing the volume the domain was unable to expand into due to merging with another domain along the [01$\bar{1}$] direction) is overestimated by the original formula and therefore in volume by that of X.

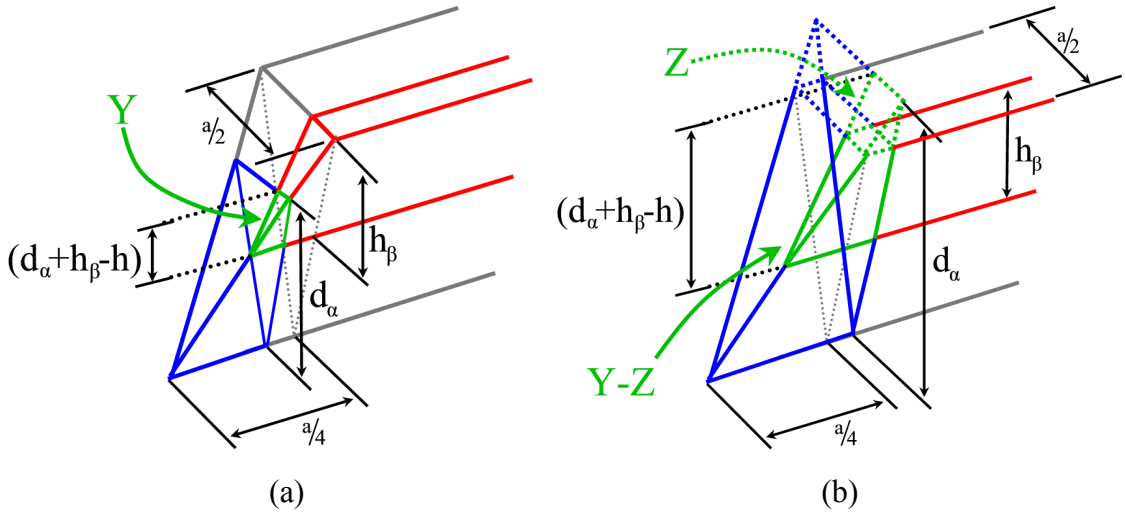


Fig. A2 Schematic of an individual domain of depth h (a) where the calculated regions of merging overlap giving a region Y and (b) where α extends past the electrode-surface resulting in Y requiring a correction of volume Z.

Figure A2a shows an example of how the volumes of α and β can overlap. It follows that a correction Y must be made to either α or β where

$$Y = \frac{1}{12}\left(d_\alpha + h_\beta - h\right)^3 - Z \qquad [A6]$$

and where Z is a correction to Y in the situation where α extends past the electrode-surface as shown in Fig. A2b:

and

$$Z = \frac{1}{4}\left(d_\alpha - h\right)^2\left[\frac{1}{3}\left(d_\alpha - h\right) + h_\beta\right] \qquad [A7]$$

It follows that the corrected formula for domain volume is

$$V_D = \frac{d^3}{6} - 2\alpha - 2\beta \qquad [A1^*]$$

$$\text{where if } a > s_a \Rightarrow \alpha = \frac{1}{6}d_\alpha^3 - X \text{ else } \alpha = 0$$

and

$$\text{if } \frac{a}{2} \geq s_b \Rightarrow \beta = \frac{1}{6}h_\beta^3 + \frac{1}{3}h_\beta^2 h - Y \text{ else } \beta = 0$$

where

$$\text{if } d_\alpha \geq h \Rightarrow X = \frac{1}{2}(d_\alpha - h)^2\left[h + \frac{d_\alpha - h}{3}\right] \text{ else } X = 0$$

$$\text{if } (d_\alpha + h_\beta) \geq h \Rightarrow Y = \frac{1}{12}(d_\alpha + h_\beta - h)^3 - Z \text{ else } Y = 0$$

and $$\text{if } d_\alpha \geq h \Rightarrow Z = \frac{1}{4}(d_\alpha - h)^2\left[\frac{1}{3}(d_\alpha - h) + h_\beta\right] \text{ else } Z = 0$$

References

1. H. Foll, J. Cartensen, S. Frey, *J. Nanomater.* 1 (2006)
2. M.I.J. Beale, J.D. Benjamin, M.J. Uren, N.G. Chew, A.G. Cullis, *J. Cryst. Growth* **73**, 622 (1985)
3. R.L. Smith, S.D. Collins, *J. Appl. Phys.* **71**, R1 (1992)
4. V. Lehmann, H. Foll, *J. Electrochem. Soc.* **137**, 653 (1990)
5. X.G. Zhang, *J. Electrochem. Soc.* **151**, C69 (2004)
6. P. Schmuki, U. Schlierf, T. Herrmann, G. Champion, *Electrochim. Acta* **48**, 1301 (2003)
7. D.N. Buckley, R.P. Lynch, N. Quill and C. O'Dwyer, *ECS Transactions* **69 (14)**, 17 (2015)
8. R. Lynch, C. O'Dwyer, D. Sutton, S. Newcomb, and D.N. Buckley, *ECS Trans.* **6,** 355 (2007)
9. C. O'Dwyer, D.N. Buckley, D. Sutton, M. Serantoni and S.B. Newcomb, *J. Electrochem. Soc.* **154** (2), H78 (2007)
10. R.P. Lynch, C. O'Dwyer, N. Quill, S. Nakahara, S.B. Newcomb and D.N. Buckley, *J. Electrochem. Soc*. **160**, D260 (2013)
11. C. O'Dwyer, D.N. Buckley, D. Sutton, M. Serantoni, and S.B. Newcomb, *J. Electrochem. Soc.,* **154**, H78 (2007)
12. N. Quill, R.P. Lynch, C. O'Dwyer and D. N. Buckley, *ECS Transactions* **50 (37)**, 131 (2012)
13. R.P. Lynch, N. Quill, C. O'Dwyer, S. Nakahara and D.N. Buckley, *Phys. Chem. Chem. Phys.* **15**, 15135 (2013)
14. R. Lynch, M. Dornhege, P. Sánchez-Bodega, H.H. Rotermund and D.N. Buckley, *ECS Trans.*, **6,** 331 (2007)

15. D. N. Buckley, C. O'Dwyer, R. Lynch, et al., Proceedings of the 41st State-of-the-Art Program on Compound Semiconductors, PV 2004-05, p.103 (ECS, 2004).
16. C. O'Dwyer, D.N. Buckley, D. Sutton and S.B. Newcomb, *J. Electrochem. Soc.* **153** (12), G1039 (2006)
17. R. Lynch, C. O'Dwyer, D.N. Buckley, D. Sutton and S. Newcomb, *ECS Transactions* **2,** 131-141 (2006)
18. D.N. Buckley, R.P. Lynch, N. Quill and C. O'Dwyer, *ECS Transactions* **69**, 17 (2015)
19. L. A. Giannuzzi and F. A. Stevie, *Micron.*, **30**, 197 (1999).
20. C. O'Dwyer, PhD Thesis: "Anodic Formation and Characterisation of Porous InP in KOH Electrolytes" Chapter 5, Supervisor: D.N. Buckley, University of Limerick (2003)
21. R.P. Lynch, N. Quill, C. O'Dwyer, M. Dornhege, H.H. Rotermund and D.N. Buckley, *ECS Transactions* **53**, 65 (2013)
22. N. Quill, C. O'Dwyer, D.N. Buckley and R.P. Lynch, *ECS Transactions* **69**, 33 (2015)
23. P. Schmuki, U. Schierf, T. Herrmann and G. Champion, *Electrochim. Acta* **48**, 1301 (2003)
24. CRC Handbook of Chemistry and Physics 86th ed.: *Physical Constants of Inorganic Compounds,* p. 4-65, D.R. Lide, Editor-in-Chief, CRC Press, New York (2005)